Supplementary Information

Embryo-scale epithelial buckling forms a propagating furrow that initiates gastrulation

Julien Fierling Alphy John Barthélémy Delorme Alexandre Torzynski
Guy B. Blanchard Claire M. Lye Grégoire Malandain Bénédicte Sanson
Jocelyn Étienne Philippe Marmottant Catherine Quilliet Matteo Rauzi

Quantifications in MuVi SPIM data

Measuring furrow propagation along the AP axis

Cross-sections were digitally made 50 µm apart along the AP axis. Furrow depth at different AP positions was measured using a dedicated point-picker ImageJ macro.

Measuring anterior pole distance

Mid-sagittal sections were digitally extracted from the time-lapses and the position of the vitelline membrane at the anterior pole and the apical position of the anterior-most blastoderm cell were recorded using the point-picker plugin. The relative apical position of the anterior-most blastoderm cell was calculated with respect to the position of the vitelline membrane at the anterior pole and this was plotted over time.

Measuring tissue shortening

Digital mid-cross and sagittal sections were obtained using ImageJ to measure tissue shortening along the DV and AP axes. Different embryos were aligned in time by keeping t0 as the frame at which cell apical area reduces to 20%. To measure tissue shortening along the AP axis, an identity cell was fixed at the half-length along the mid-sagittal section. Cells located 100 µm anteriorly and posteriorly from this point were marked and their distance from the identity cell was measured over time along the embryo surface. To measure tissue

shortening along the DV axis, an identity cell was fixed at the midline of cross-sectional images at the ventral side. The distance along the embryo surface of the two cells located on opposite sides four cells away from the identity cell was then measured over time.

Recoil velocity

To measure actomyosin network recoil after ablation, the point-picker plugin was used to follow the cut end. Distance moved by the network after ablation was plotted against time and the maximum recoil velocity was measured by calculating the first derivative.

Curvature analysis

An ImageJ macro was developed to measure the radius (R) of a circle generated from three consecutive points. The curvature was calculated as 1/R and was plotted against time. Curvature of the mesoderm tissue was measured both along the AP and DV axes. A convex curvature is given by a positive and a concave curvature is given by a negative value.

3D image segmentation and analysis

Mesodermal cells were segmented and tracked by inter-registration based on iterative projections of segmentations from one time point to another using the ASTEC algorithm (1). Morphological data were extracted and analyzed using Python. ImageJ dedicated macros were used for image treatment and the 3D Viewer plugin for rendering (2).

Brief introduction to the strain and stress tensors

We would like to remind the reader of a few facts concerning tensors in mechanics.

Both the strain and the stress within the material need to be represented by second-order tensor fields, that is, that for each point within the material there is a local tensor associated. For a linear elastic material, the stress and strain tensors are linearly related to one another, see Eq. 2 below.

It is not in itself necessary that the variations of these tensors in space are smooth (that is, that for two given points in the material close enough, the tensors have small difference), but some smoothness arises

from the mechanical balance that the stress tensor has to obey (which imposes that some derivatives of the stress tensor are small) and, as a result, for the strain tensor through Eq. 2.

An intuitive way to understand what the stress tensor $\boldsymbol{\sigma}(\boldsymbol{r})$ corresponds to is to realise that it predicts how the material would move if a cut of infinitesimal length ℓ was done in the given location $\boldsymbol{r}$. This is an idealised version of the biophysical experiment of laser dissection, where the cut length would be infinitesimal and the cut width exactly zero. For simplicity we treat it in the case of a two-dimensional material, which is the case of our model. Let us denote by the unit vector $\boldsymbol{e}$ the direction orthogonal to the laser dissection. Note of course that $-\boldsymbol{e}$ is also a unit vector orthogonal to the laser direction, pointing to the other side. To fix ideas and without loss of generality, let's define $\boldsymbol{e}$ as the right-pointing vector, and $-\boldsymbol{e}$ as the left-poiting vector. The dot product of the stress tensor with the direction vector, $\boldsymbol{f} = \boldsymbol{\sigma} \cdot \boldsymbol{e}$, is the vector of (lineic[1]) force that the material situated to the right of the cut exerts on the line of cut, and $-\boldsymbol{f} = \boldsymbol{\sigma} \cdot (-\boldsymbol{e})$ the equal and opposite vector of force that the material situated to the left of the cut exerts on the line of cut. These equal and opposite forces pre-exist the cut: before a cut is done, the material is in mechanical balance because there is continuity of the material across the cut-line and the forces cancel. Once the cut is made, this is not the case anymore, and if one would want to maintain the material in its original shape in spite of the cut, one would have to "hold" both sides with respectively a force $-\boldsymbol{f}$ applied to the one to the right and $\boldsymbol{f}$ applied to the one on the left. If there is nothing to "hold" in place the sides of the cut, there will be motion: in a first approximation, if there is some frictional resistance to it, the initial velocity with which the sides of the cut open will be proportional to $\boldsymbol{f}$ and $-\boldsymbol{f}$ in the right and left side respectively.

The stress is said isotropic if the magnitude of the force $\boldsymbol{f}$ is the same for any cut direction $\boldsymbol{e}$. In this case, the vector $\boldsymbol{f}$ is always perfectly aligned with $\boldsymbol{e}$. If the stress is not isotropic, then for an infinitesimal cut it can be shown that there are exactly two directions $\boldsymbol{e}_1$ and $\boldsymbol{e}_2$ for which $\boldsymbol{f}_1 = \boldsymbol{\sigma} \cdot \boldsymbol{e}_1$ and $\boldsymbol{f}_2 = \boldsymbol{\sigma} \cdot \boldsymbol{e}_2$ are respectively aligned with $\boldsymbol{e}_1$ and $\boldsymbol{e}_2$. For any other direction $\boldsymbol{e}$ of the cut, the vector $\boldsymbol{f}$ will not be exactly along $\boldsymbol{e}$: the component of $\boldsymbol{f}$ orthogonal to $\boldsymbol{e}$ is called the shear force. The directions $\boldsymbol{e}_1$ and $\boldsymbol{e}_2$ are called the principal directions of the stress, they are orthogonal to one another. Since they are unit vectors, it is sufficient to give one orientation angle to define completely $\boldsymbol{e}_1$ and $\boldsymbol{e}_2$: for instance, in our case, giving the angle θ of $\boldsymbol{e}_1$ with the AP direction in the mesoderm describes the principal directions of the stress completely. It can be shown

[1] that is, the force per unit length, the total force being $\ell \boldsymbol{f}$, product of the lineic force with the length of the cut. For simplicity, we will name "force" the lineic force in what follows.

that the stress tensor can then be written as $\boldsymbol{\sigma} = \sigma_1 \boldsymbol{e}_1 \otimes \boldsymbol{e}_1 + \sigma_2 \boldsymbol{e}_2 \otimes \boldsymbol{e}_2$, where $\otimes$ is the dyadic product and $\sigma_1,\ \sigma_2$ are called the principal stresses. As a result, the stress tensor for our case of a two-dimensional material, it has three degrees of freedom, $\sigma_1,\ \sigma_2$ and θ, and it can thus be represented as an ellipse or as the cross formed by the two main axes of an ellipse on the surface of the material (see e.g. Supp. Fig. 1b) with the caveat that either or both of $\sigma_1,\ \sigma_2$ can be negative (which corresponds to compressive stress in either or both direction, whereas a positive sign denotes tensile stress). The trace of the stress tensor can then easily be expressed as $\sigma_1 + \sigma_2$, it is one of the invariants of the tensor and is convenient to represent a level of stress with a scalar (see e.g. Fig 2b).

The strain tensor is described in details in the context of morphogenesis by (3).

Numerical simulations

Geometry of the elastic surface of the model

Following (4), we approximate the initial embryo shape by a closed surface of equation:

$$\Gamma_0 = \left\{ \left(\frac{x}{R_{AP}}\right)^2 + \left(\frac{y}{R_{DV}}\right)^2 + \left(\frac{z}{R_{DV}} - Z_p \left(\frac{x}{R_{AP}}\right)^2\right)^2 = 1 \right\}$$

This describes a prolate ellipsoid, with circular cross-sections. The mid-cross-section at $x = 0$ is a circle of radius R_{DV} centered at $(x, y, z) = (0, 0, 0)$. For a positive parameter Z_p, this ellipsoid is bent with the center of cross-sections offset towards increasing z as $|x|$ increases. In particular, the poles along the long axis are at the positions $(x, y, z) = (\pm R_{AP}, 0, Z_p)$.

As in (4), we choose $R_{AP} = 3R_{DV}$ and $Z_p = 0.45$, which defines the shape corresponding to the initial equilibrium configuration of the elastic surface in terms of in-plane stress. While all calculations are done in nondimensional units of R_{DV}, the dimensional counterparts of all quantities are then calculated with $R_{DV} =$ 90 µm.

The elastic surface $\Gamma(\sigma_\mathrm{a})$ is then defined as the surface of minimal elastic energy for a given pre-stress field σ_a. The spatial dependence of σ_a is described in the main text, the corresponding rheology is described in what follows.

Additionally, two constraints are applied to the configuration of the elastic surface Γ. First, it encloses

a constant volume independent of σ_a and equal to the initial volume of Γ_0. This models the fact that the permeability of the apical surface of the epithelium is low, such that water fluxes across it are assumed to be zero during the process of initial furrow formation. This gives rise to pressure forces which are dependent on σ_a and are of uniform magnitude in space. Second, Γ is itself enclosed in an undeformable vitelline membrane. The vitelline membrane is defined as a closed surface Γ_V parallel to the initial elastic surface Γ_0, at a distance $2.5 \times 10^{-3} R_{DV} \simeq 0.2$ µm towards the exterior. Non-interpenetration of the elastic surface with the vitelline membrane is simulated by Surface Evolver constraint algorithm (5), a penalty method based on a level set function ensuring that the elastic surface is in the interior side of Γ_V.

Elastic model

The deformation of an elastic layer of non-vanishing thickness can be modelled using a surface with two local additive contributions: bending and in-plane deformation (6, 7).

The bending surface energy density writes $\frac{1}{2}\kappa\left(c - c_0\right)^2$ where κ is the bending modulus of the surface, $c = \frac{1}{R_1} + \frac{1}{R_2}$ its mean curvature (R_i are the principal algebraic curvature radii), and c_0 the (local) intrinsic curvature, taken to be the initial one in this work (6, 8).

We now proceed to describe the part of the surface energy density due to in-plane deformation. In a continuum description of in-plane deformations, the gradient deformation matrix $\mathbf{F}^c$, with $F^c_{ij} = \frac{\partial X_i}{\partial x_j}$ where (X_1, X_2), describes the deformed position of a material point initially at the (x_1, x_2) position (the indices stand for any two coordinates describing a surface), allow to define the right Cauchy-Green deformation tensor $\left(\mathbf{F}^c\right)^T\mathbf{F}^c$ and the Lagrangian finite strain tensor $\boldsymbol{\epsilon} = \left(\left(\mathbf{F}^c\right)^T\mathbf{F}^c - \mathbf{I}\right)/2$, a widely used measure of how a material piece of surface locally differs before and after deformation.

The elasticity of the surface is described by the Hookean model, where the (locally) in-plane stress tensor $\boldsymbol{\sigma}$ is linked to the (locally) in-plane strain tensor $\boldsymbol{\epsilon}$. The model surface is considered as isotropic in plane, which allows to describe full elasticity using only two parameters, the 2D Young modulus Y_{2D} and the 2D Poisson ratio ν_{2D}. The surface energy density of in-plane deformation in this model can be expressed in two

different useful forms:

$$
\begin{aligned}
e_{def} &= \frac{Y_{2D}}{2(1+\nu_{2D})}\left[\mathrm{Tr}(\boldsymbol{\epsilon}^2) + \frac{\nu_{2D}}{1-\nu_{2D}}(\mathrm{Tr}\boldsymbol{\epsilon})^2\right] \\
&= \frac{\chi_{2D}}{2}(\mathrm{Tr}\boldsymbol{\epsilon})^2 + \mu_{2D}\left(\mathrm{Tr}(\boldsymbol{\epsilon}^2) - \frac{1}{2}(\mathrm{Tr}\boldsymbol{\epsilon})^2\right)
\end{aligned} \tag{1}
$$

where χ_{2D} and μ_{2D} are, respectively, the 2D compression and shear moduli:

$$
\chi_{2D} = \frac{Y_{2D}}{2(1-\nu_{2D})} \qquad \mu_{2D} = \frac{Y_{2D}}{2(1+\nu_{2D})}
$$

In-plane stresses write:

$$
\boldsymbol{\sigma} = \chi_{2D}(\mathrm{Tr}\boldsymbol{\epsilon})\mathbf{P} + 2\mu_{2D}\left(\boldsymbol{\epsilon} - \frac{1}{2}(\mathrm{Tr}\boldsymbol{\epsilon})\mathbf{P}\right) \tag{2}
$$

with $\mathbf{P} = \mathbf{I} - \boldsymbol{n}\otimes\boldsymbol{n}$ the projection tensor along the surface.

We nondimensionalise the parameters with $\tilde{\chi}_{2D} = \chi_{2D}R_{DV}^2/\kappa$ and $\tilde{\mu}_{2D} = \mu_{2D}R_{DV}^2/\kappa$. All figures are shown for the choices $\tilde{\chi}_{2D} = 50$ and $\nu_{2D} = 0$.

Numerical approach

We describe here the approach generally used in the Surface Evolver (5). Although these implementation details are not specific to our approach, they are necessary to introduce the numerical technique for simulation pre-strain in the next paragraph.

In a finite element description, $\mathbf{F}^c$ is approximated locally by $\mathbf{F}$, the matrix of the linear transformation from the unstrained to the strained facet, written in a local basis. Let $\mathbf{S} = [S_1, S_2]$ be the 2×2 matrix formed by any 2 sides of the unstrained facet ABC,

$$
\mathbf{S} = \begin{bmatrix} x_B - x_A & x_C - x_A \\ y_B - y_A & y_C - y_A \end{bmatrix},
$$

and $\mathbf{W}$ the corresponding matrix of the same facet in the deformed configuration. Then $\mathbf{W} = \mathbf{FS}$ which rewrites $\mathbf{F} = \mathbf{WS}^{-1}$. With $\mathbf{F}^T = \left(\mathbf{S}^{-1}\right)^T\mathbf{W}^T$, one gets the numerical implementation for approximating the

Lagrangian finite strain tensor in each facet of the finite element mesh:

$$\mathbf{E} = \frac{1}{2}\left(\left(\mathbf{S}^{-1}\right)^T \mathbf{W}^T \mathbf{W} \mathbf{S}^{-1} - I\right)$$

Note that this expression is invariant with respect to permutations between A, B and C.

In practice, since $\boldsymbol{\epsilon}$ appears in Eq. 1 only through $\mathrm{Tr}\left(\boldsymbol{\epsilon}^2\right)$ and $\mathrm{Tr}\,\boldsymbol{\epsilon}$, one can use an alternative representation of the strain, namely $\mathbf{E}^* = \left(\mathbf{S}^T\right)^{-1} \mathbf{E} \mathbf{S}^T$, because due to matrix properties, $\mathrm{Tr}\,\mathbf{E}^* = \mathrm{Tr}\,\mathbf{E}$ and $\mathrm{Tr}\left(\mathbf{E}^{*2}\right) = \mathrm{Tr}\left(\mathbf{E}^2\right)$.

This definition is equivalent to $\mathbf{E}^* = \frac{1}{2}\left(\mathbf{W}^T \mathbf{W} \mathbf{S}^{-1} \left(\mathbf{S}^{-1}\right)^T - \mathbf{I}\right)$, or $\mathbf{E}^* = \frac{1}{2}\left(\mathbf{G}_W \left(\mathbf{G}_S\right)^{-1} - \mathbf{I}\right)$, where $\mathbf{G}_W = \mathbf{W}^T \mathbf{W}$ and $\mathbf{G}_S = \mathbf{S}^T \mathbf{S}$ are the (real and symmetric, hence diagonalisable) Gram matrices of, respectively, the strained and unstrained facets. Since Gram matrices, that make only intervene the square lengths and the scalar product of the two sides choosen to determine the facets, are easy to calculate from side lengths only, the alternative definition E^* is preferred in the minimisation algorithm used for the equilibrium situations (5).

Pre-strain and pre-stress

Pre-strain corresponds to a reduction of the equilibrium configuration area. In order to apply pre-strain in a given facet, we multiplied the Gram matrix of the unstrained facet by a factor $\gamma < 1$ (which amounts to multiply the dimensions of the equilibrium configuration of the facet by $\sqrt{\gamma}$):

$$\mathbf{G}_S^\gamma = \gamma \mathbf{G}_S$$

This approach can be compared to morphoelasticity, see (9).

The alternative deformation tensor hence becomes:

$$\begin{aligned}\mathbf{E}_\gamma^* &= \frac{1}{2}\left(\frac{1}{\gamma}\mathbf{G}_W \left(\mathbf{G}_S^\gamma\right)^{-1} - \mathbf{I}\right) \\ &= \frac{1}{\gamma}\mathbf{E} - \frac{\gamma - 1}{2\gamma} I\end{aligned}$$

The trace is easily calculated:

$$\mathrm{Tr}(\mathbf{E}_\gamma^*) = \frac{1}{\gamma}\mathrm{Tr}\mathbf{E} - \frac{(\gamma - 1)}{\gamma}$$

The stress thus becomes:

$$\begin{aligned}\sigma_\gamma &= \chi_{2D}(\mathrm{Tr}\mathbf{E}^*_\gamma)I + 2\mu_{2D}\left(\mathbf{E}^*_\gamma - \frac{1}{2}(\mathrm{Tr}\mathbf{E}^*_\gamma)\mathbf{I}\right)\\ &= \chi_{2D}\left[\frac{1}{\gamma}\mathrm{Tr}\mathbf{E} - \frac{(\gamma-1)}{\gamma}\right]\mathbf{I} + 2\mu_{2D}\left(\left[\frac{1}{\gamma}\mathbf{E} - \frac{\gamma-1}{2\gamma}\mathbf{I}\right] - \frac{1}{2}\left[\frac{1}{\gamma}\mathrm{Tr}\mathbf{E} - \frac{(\gamma-1)}{\gamma}\right]\mathbf{I}\right)\\ &= \frac{\chi_{2D}}{\gamma}\left[\mathrm{Tr}\mathbf{E} - (\gamma-1)\right]\mathbf{I} + 2\frac{\mu_{2D}}{\gamma}\left(\mathbf{E} - \frac{1}{2}(\mathrm{Tr}\mathbf{E})\mathbf{I}\right)\end{aligned}$$

Area pre-strain is thus equivalent to an isotropic pre-stress $\sigma_a = \chi_{2D}\frac{\gamma-1}{\gamma}$. Note that the apparent elastic moduli of the material are also increased by a factor $1/\gamma$, due to the fact that their equilibrium configuration is of dimensions $1/\gamma$-fold smaller than their intial configuration, with respect to which strain is calculated.

References

1. Guignard, L., Fiúza, U.-M., Leggio, B., Laussu, J., Faure, E., Michelin, G., Biasuz, K., Hufnagel, L., Malandain, G., Godin, C. & Lemaire, P. Contact area–dependent cell communication and the morphological invariance of ascidian embryogenesis. *Science* **369,** eaar5663. doi:10.1126/science.aar5663 (6500 2020).

2. Schmid, B., Schindelin, J., Cardona, A., Longair, M. & Heisenberg, M. A high-level 3D visualization API for Java and ImageJ. *BMC Bioinformatics* **11,** C213. doi:10.1186/1471-2105-11-274 (1 2010).

3. Blanchard, G. B., Kabla, A., Schultz, N., Butler, L., Sanson, B., Gorfinkiel, N., Mahadevan, L. & Adams, R. Tissue tectonics: morphogenetic strain rates, cell shape change and intercalation. *Nature Methods* **6,** 458–464 (2009).

4. Dicko, M., Saramito, P., Blanchard, G. B., Lye, C. M., Sanson, B. & Étienne, J. Geometry can provide long-range mechanical guidance for embryogenesis. *PLoS Comput Biol* **13,** e1005443. doi:10.1371/journal.pcbi.1005443 (3 2017).

5. Brakke, K. A. The Surface Evolver. *Experimental Mathematics* **1,** 141–165. doi:10.1080/10586458.1992.10504253 (2 1992).

6. Landau, L. D. & Lifshitz, E. F. *Theory of elasticity Course of theoretical physics* **7** (Pergamon Press, 1970).

7. Ben Amar, M. & Pomeau, Y. Crumpled paper. *Proc. R. Soc. Lond. A* **453,** 729–755. doi:10.1098/rspa.1997.0041 (1959 1997).

8. Helfrich, W. Elastic properties of lipid bilayers: Theory and possible experiments. *Z. Naturforsch.* **28C,** 693–793 (1973).

9. Goriely, A. *The Mathematics and Mechanics of Biological Growth* (Springer, 2017).

Supplementary Movies

Supplementary movie 1: Time-lapse showing actomyosin network recoil after IR fs laser dissection and eventual actomysin network recovery. Scale bar 10 μm.

Supplementary movie 2: Time-lapse showing mesoderm internalization failure as a consequence of periodic ventral tension inhibition. The ventral actomyosin network is periodically dissected using a IR fs laser over a grid patterned ROI. Scale bar 10 μm.

Supplementary movie 3: 3D rendering of segmented apical surfaces of ventral cells. Scale bar 50 μm.

Supplementary movie 4: Time-lapse showing digital sections along the sagittal plane (top) and along different cross-section planes at different AP positions in a wild-type embryo. Scale bar 100 μm.

Supplementary movie 5: Time-lapse showing different cross-section planes at different AP positions in a wild-type embryo and eye guide highlighting furrow apex position. Scale bar 100 μm.

Supplementary movie 6: Time-lapse showing digital sections along the sagittal plane (top) and along different cross-section planes at different AP positions in a slam-dunk- embryo. Scale bar 100 μm.

Supplementary movie 7: Time-lapse showing ventral tissue flattening along a line connecting cauterized loci. Scale bar 100 μm.

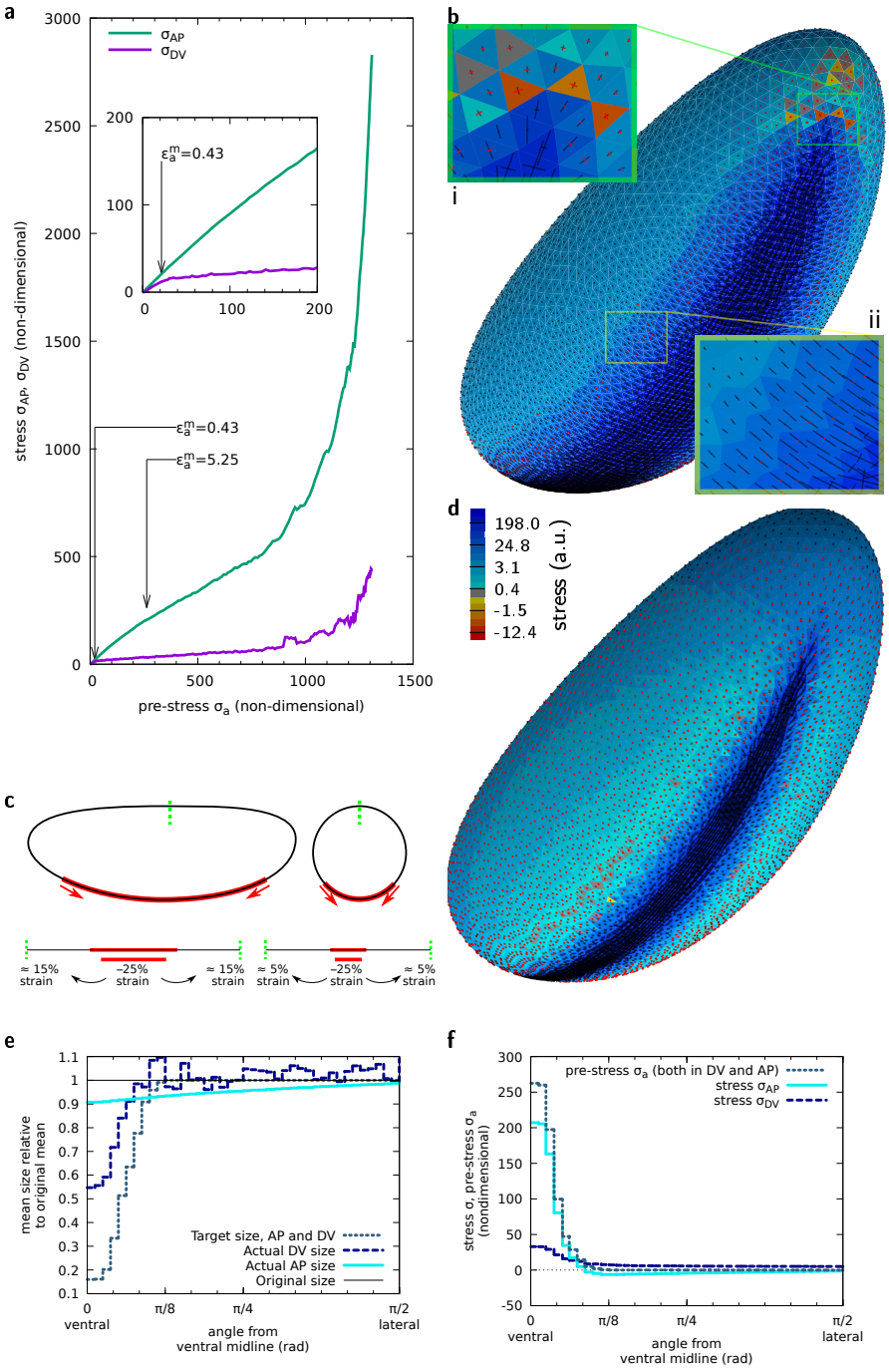

Supplementary Figure 1: (**a**) Evolution of AP and DV stresses at the ventral midline as a function of the pre-stress σ_a. (**b**) Principal stresses in each facet for midline pre-strain $\varepsilon_a^m = 0.43$. Black segments, positive principal stress (tensile); red segments, negative principal stress (compressive) along the corresponding directions. Facet colours, sum of the principal stresses, see **d** for colour code. Inserts (i) and (ii), 3× zoom of the regions outlined in white and in yellow. In (ii), tensor components are further enlarged by a factor 2. (**c**) Representation in sagittal and transverse sections of an example 25% strain in the ventral region and of the strain it implies in other regions if the embryo shape is unchanged. (**d**) Principal stresses in each facet for midline pre-strain $\varepsilon_a^m = 5.25$. Same colour code as **b**. (**e**) Same as Fig. 2a but for $\varepsilon_a = 5.25$. (**f**) Same as Fig. 2c but for $\varepsilon_a = 5.25$.

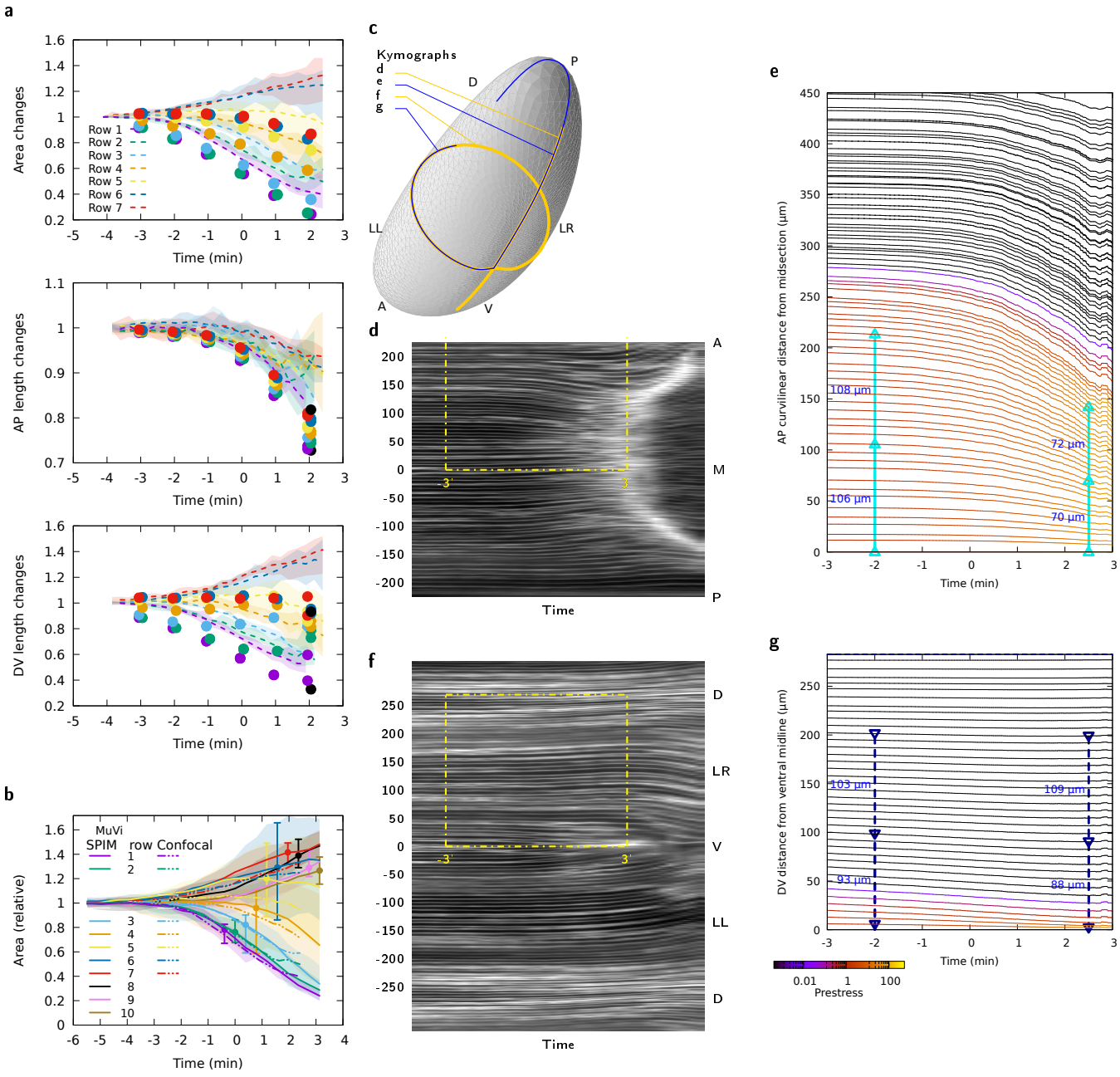

Supplementary Figure 2: (**a**) Time evolution of apical area, AP and DV sizes of cells at different distances from the midline, in confocal experiments (lines) and simulations (symbols). (**b**) Time evolution of apical area of cells in MuVi SPIM and confocal experiments. (**c**) Localisation of kymographs of panels **d**–**g** on the apical surface of the embryo. (**d**) Kymograph of membrane signal in MuVi SPIM along AP (mid-sagittal line). M, mid; A, anterior; P, posterior, coordinates from mid-transverse plane in µm. Yellow box delineates the zone also shown in panel **e**. (**e**) Same as **d** in simulations, with colour coded pre-stress value (see colour bar in **g**) and quantification of the decrease of length between mid-transverse point and points marked with symbols. (**f**) Kymograph of membrane signal in MuVi SPIM along DV (mid-transverse line). V, ventral; LR, lateral right; LL, lateral left; D, dorsal, coordinates from the ventral midline in µm. (**g**) Same as **f** in simulations.

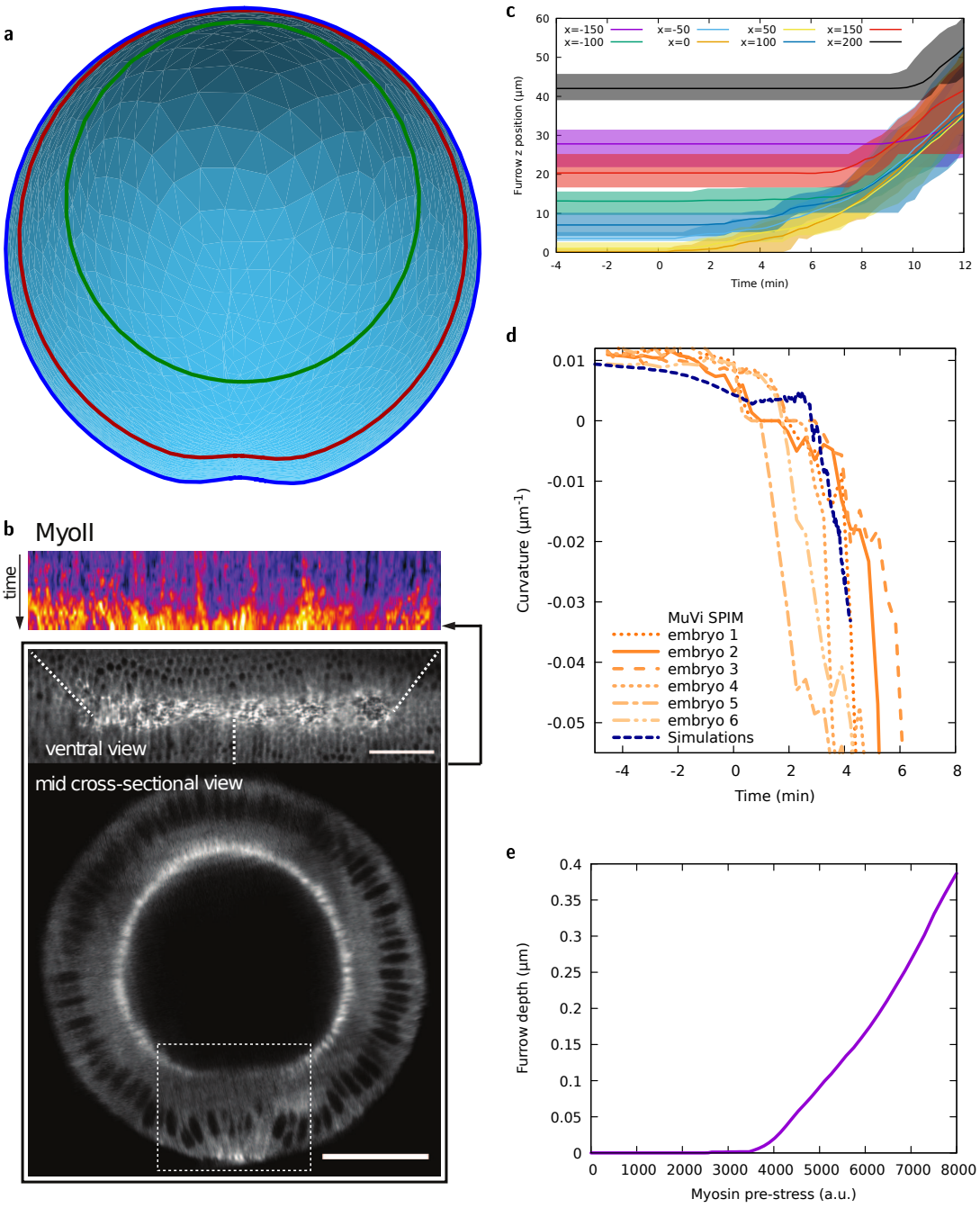

Supplementary Figure 3: (**a**) See-through view of embryo shape in simulations at $t = 4'12''$ from the posterior end. (**b**) Top, kymograph showing MyoII accumulation along the AP axis. Mid and bottom, ventral and mid-transverse view of the embryo before folding, respectively. Scale bars 50 µm. (**c**) Ventral furrow apex position at different AP positions. Lines represent medians and shaded areas the interval between min and max values. The analysis was performed on 6 embryos. Negative and positive x values indicate more anterior and more posterior positions, respectively. (**d**) Curvature of the ventral tissue along the DV axis as a function of time, with individual data from $n = 6$ MuVi SPIM embryos. (**e**) Depth of the ventral furrow as a function of the pre-stress σ_a applied.